Journal of Materials Chemistry A

Accepted Manuscript

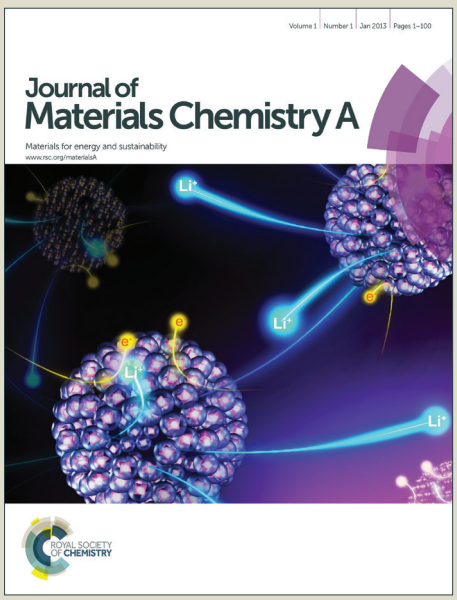

ROYAL SOCIETY OF CHEMISTRY

www.rsc.org/materialsA

Cite this: DOI: 10.1039/c0xx00000x

www.rsc.org/xxxxxx

ARTICLE TYPE

Insight into an unusual lanthanum effect on the oxygen reduction reaction activity of Ruddlesden-Popper-type cation-nonstoichiometric $La_{2-x}NiO_{4+\delta}$ (x=0~0.1) oxides

Yubo Chen,[a] Baoming Qian,[a] Guangming Yang,[a] Dengjie Chen[b] and Zongping Shao[a,c]

Received (in XXX, XXX) Xth XXXXXXXXX 20XX, Accepted Xth XXXXXXXXX 20XX
DOI: 10.1039/b000000x

The creation of cation deficiency in the Ln-site of some Ruddlesden-Popper-type $Ln_2NiO_{4+\delta}$ oxides (Ln=Pr, Nd) can promote oxygen reduction activity of the materials at elevated temperature; however, La-nonstoichiometric $La_2NiO_{4+\delta}$ materials have been reported to behave differently. In this study, a series of $La_{2-x}NiO_{4+\delta}$ (x=0~0.1) materials was synthesized and systematically characterized to obtain information regarding the origin of their different electrochemical behavior. Based on XRD and HR-TEM characterizations, a high-order $La_3Ni_2O_7$ phase was detected even in the case of slight La deficiency (x=0.02), and its content increased with increasing degree of La nonstoichiometry, suggesting unfavorable formation of cation deficiency in $La_{2-x}NiO_{4+\delta}$. Such a high-order Ruddlesden-Popper-type oxide typically improves the oxygen reduction activity; however, reduced activity with increasing La nonstoichiometry for the samples was actually detected based on symmetrical cell tests. In-depth impedance analysis revealed that the deteriorated electrochemical performance was mainly due to the inferior charge transfer process occurring at the electrode/gas interface and/or oxygen ions transferring through the electrolyte/electrode interface. The microstructures of the La-deficient $La_{2-x}NiO_{4+\delta}$ electrodes were then carefully observed using SEM. Both the electrode particle interconnection and the adhesion of the electrode layer to the electrolyte were poor, which was related to the poor sintering ability of the high-order $La_3Ni_2O_7$ phase that deteriorated the electrode performance.

Introduction

To accelerate the commercialization of solid oxide fuel cells (SOFCs), reducing the operation temperature from 850~1000 °C to the intermediate-to-low temperature range of 500~850 °C is highly desired, which may lead to increased long-term operational stability and reduced costs associated with the fabrication and operation of SOFCs and make them economically more competitive.[1,2] Poor electrochemical performance of SOFCs at reduced temperatures, which is strongly related to the insufficient oxygen reduction reaction (ORR) activity of conventional cathodes, is the main obstacle in lowering the operation temperature of SOFCs.[3] Therefore, tremendous efforts have been devoted to searching for alternative electrode materials with improved performance for ORR at reduced temperature. During the past years, many mixed conducting perovskite or perovskite-related oxide materials for ORR in SOFCs, such as $Ba_{0.5}Sr_{0.5}Co_{0.8}Fe_{0.2}O_{3-\delta}$ and $PrBaCo_2O_{5+\delta}$, have been developed.[4,5] In these perovskite or related materials, metal ions with lower valence states, especially alkaline earth elements, must be doped into the crystal lattice to form a sufficient oxygen hypo-stoichiometry. Unfortunately, these alkaline earth metal element-containing materials have high sensitivity toward impurities (Cr species and CO_2) from the surrounding atmosphere.[6-9] The segregation of the alkaline earth metal elements from the bulk of these materials on their catalytic activity is another thing should be concerned, as the conclusions about the influence of this cation segregation are controversial.[10-14] Thus, their use in practical SOFCs is limited. Therefore, the development of new materials with outstanding performance (activity and stability) for ORR is still urgently needed.

The Ruddlesden-Popper type of metal oxides, a series of composite oxides with the general formula $A_{n+1}B_nO_{3n+1}$ (n=1, 2, 3…), has recently attracted attention as alternative cathode materials for SOFCs. In a $A_{n+1}B_nO_{3n+1}$ material, n ABO_3 perovskite layers are sandwiched between two AO rock-salt layers and are arranged along the c-axis. The first members of the Ruddlesden-Popper series take the K_2NiF_4 structure.[15,16] In fact, most common Ln_2NiO_4 (Ln=lanthanide) oxides take such lattice structure. These oxides are very intriguing because of their oxygen-ion-conducting capability through intrinsic oxygen without the necessity of alkaline earth metals.[17] Moreover, these layered materials also possess some other important advantages, including acceptable electronic conductivity, moderate thermal

Table 1 The refined results of the diffraction patterns of La-deficient $La_{2-x}NiO_{4+\delta}$ phases.

Sample	$La_2NiO_{4+\delta}$	$La_{1.98}NiO_{4+\delta}$		$La_{1.95}NiO_{4+\delta}$		$La_{1.90}NiO_{4+\delta}$		$La_3Ni_2O_7$
	La_2NiO_4 Fmmm	La_2NiO_4 Fmmm	$La_3Ni_2O_7$ Fmmm	La_2NiO_4 Fmmm	$La_3Ni_2O_7$ Fmmm	La_2NiO_4 Fmmm	$La_3Ni_2O_7$ Fmmm	$La_3Ni_2O_7$ Fmmm
a (Å)	5.460(1)	5.462(9)	5.41(3)	5.463(4)	5.39(2)	5.463(3)	5.38(1)	5.391(7)
b (Å)	5.464(8)	5.467(5)	5.45(3)	5.465(7)	5.44(4)	5.466(1)	5.42(4)	5.446(8)
c (Å)	12.682(8)	12.688(6)	20.6(3)	12.685(2)	20.4(8)	12.686(1)	20.4(6)	20.52(2)
V ($Å^3$)	378.4(4)	378.9(9)	60(9)	378.8(0)	60(1)	378.8(4)	59(7)	602.(7)
Ref.[a] (wt. %)	/	97.87	2.13	92.66	7.34	83.81	16.19	/
Theo.[b] (wt. %)	/	96.75	3.25	91.77	8.23	83.22	16.78	/
Rp	3.77%	6.19%		6.74%		7.74%		8.63%
Rwp	5.31%	4.75%		5.09%		6.17%		6.57%
X^2	4.440	2.159		3.129		3.975		4.414

[a] Refined mass ratio of La_2NiO_4 and $La_3Ni_2O_7$

[b] Theoretical mass ratio of La_2NiO_4 and $La_3Ni_2O_7$

expansion (~12×10^{-5} K^{-1}) and promising electro-catalytic activity.[18,19]

More recently, some A-site cation-deficient Ln_2NiO_4 oxides have been further developed, which showed great potential as oxygen reduction electrodes in SOFCs.[20-27] For example, at 500 °C, it was reported that a Pr-deficient $Pr_{1.9}NiO_{4+\delta}$ material exhibited a very high oxygen chemical diffusion coefficient (D_{chem}=~10^{-4} cm^2 s^{-1}) and surface exchange constant (k_{chem}=~10^{-3} cm s^{-1}), which are approximately one order of magnitude higher than those of a stoichiometric $Pr_2NiO_{4+\delta}$. It was believed that the Pr vacancies in the sub-lattice decreased the activation barrier for oxygen diffusion.[23] Similar results were also observed in Nd-deficient Nd_2NiO_4.[24,25] The single phase A-site deficient material $La_{2-x}NiO_{4+\delta}$ (x=0.02~0.05) was also reported.[20,21] However, unlike Pr- or Nd-deficient $Ln_{2-x}NiO_{4+\delta}$ materials, the La deficiency did not result in an electrochemical performance improvement for $La_{2-x}NiO_{4+\delta}$. Instead, the bulk diffusion and the surface exchange properties were reported to be inferior to that of a stoichiometric $La_2NiO_{4+\delta}$.[20] This result suggests that a systematic examination of the La deficiency with a wider scope regarding the properties and electrochemical performance of $La_{2-x}NiO_{4+\delta}$ electrocatalysts for ORR is necessary to clarify such abnormal behavior. The knowledge obtained from these related studies is highly helpful for the further development of Ruddlesden-Popper metal oxides as electrocatalysts for ORR at elevated temperatures.

Based on the above considerations, in this study, a series of $La_{2-x}NiO_{4+\delta}$ (x=0.0-0.1) materials was synthesized by a sol-gel process, and the phase compositions of the oxides with different La deficiency were systematically analyzed. The electrochemical performance of the materials for ORR at intermediate temperatures was then studied by electrochemical impedance based on symmetrical cell tests. The effect of La deficiency on the activity for ORR was analyzed and explained based on the phase compositions and morphologies of the oxides.

Results and discussion

Fig. 1 shows the X-ray diffraction patterns of various $La_{2-x}NiO_{4+\delta}$ materials with different degrees of La nonstoichiometry (x=0.0, 0.02, 0.05 and 0.1). For comparison, the diffraction pattern of $La_3Ni_2O_7$/$La_{1.5}NiO_{4+\delta}$ is also presented.

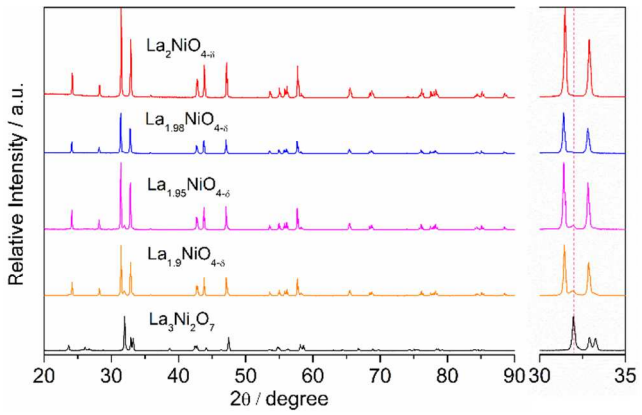

Figure 1 The X-ray diffraction patterns of various $La_{2-x}NiO_{4+\delta}$ materials with different La deficiency degrees (x=0.0, 0.02, 0.05 and 0.1).

Compared with the cation-stoichiometric $La_2NiO_{4+\delta}$, a distinct impurity peak is observed at the 2-theta value of approximately 31.9 ° for all of the La-deficient samples in their XRD patterns, even for the $La_{1.98}NiO_{4+\delta}$ sample with only slight La deficiency (x=0.02). The presence of impurity phase(s) implies the difficulty in the creation of a single-phase La-deficient $La_{2-x}NiO_{4+\delta}$. On the other hand, the intensity of the peaks belonging to the impurity phase increased monotonously with increased La nonstoichiometry, and the positions of these impurity peaks were similar to those of the as-synthesized $La_3Ni_2O_7$ phase. In an earlier study, a thermodynamic calculation of the stable phase composition of the ternary La-Ni-O system was conducted, and the results are summarized in Fig. S1. The formation of high-order $La_3Ni_2O_7$ and $La_4Ni_3O_{10}$ composites was preferred in the case of lanthanum nonstoichiometric $La_{2-x}NiO_{4+\delta}$.[28] From these results, it seems that the formation of La-site cation-deficient $La_2NiO_{4+\delta}$ is unlikely. Instead, the creation of higher-order RP phase(s) is/are preferred by introducing La deficiency. Indeed, in an earlier study, P. Odier et al. found that a higher-order Ruddlesden-Popper-type phase ($La_3Ni_2O_7$) formed when the atomic ratio of La/Ni was lower than 2.[29]

To obtain further information regarding the phase compositions of the various as-synthesized $La_{2-x}NiO_{4+\delta}$ materials, their experimental X-ray diffraction patterns were subjected to

Rietveld refinement. At room temperature, stoichiometric $La_2NiO_{4+\delta}$ oxide typically exhibits two different phase structures: a tetragonal phase (space group: I *4/mmm*) and an orthorhombic phase (space group: F *mmm*), as reported by different authors.[30,31] Herein, both structures were tried in the refinement of the diffraction patterns of $La_2NiO_{4+\delta}$, and the corresponding refined diffraction patterns and reliability factors are listed in Fig. S2. The refinement using an orthorhombic structure shows better accuracy, which can also be observed from the high-angle fitting patterns shown in the insets in Fig. S2. Therefore, the orthorhombic phase structure (F *mmm*) was confirmed for the La cation-stoichiometric $La_2NiO_{4+\delta}$ sample at room temperature, which was then chosen for the following refinements. For the refinement of the diffraction patterns of the La-nonstoichiometric $La_{2-x}NiO_{4+\delta}$ samples, a two-phase model, which contained a $La_2NiO_{4+\delta}$ orthorhombic phase and a $La_3Ni_2O_7$ phase (F *mmm*), was applied. The refined results are listed in Table 1, and the fitting patterns are given in Fig. S3 and the variation of the lattice parameters of the primary $La_2NiO_{4+\delta}$ phase in these samples is drawn in Fig. S4. It can be found that their lattice parameters vary in a very small magnitude, and the cell volumes are close to each other. This phenomenon suggests that the actual La deficiency in these samples is very small. Thus, it is reasonable to assume that the $La_2NiO_{4+\delta}$ phase could not suffer from any La deficiency. This result is in good agreement with the conclusion from the thermodynamic calculations. Then, the theoretical mass ratios of the $La_2NiO_{4+\delta}$ phase in these materials were calculated based on the above assumption. The refined mass ratios of $La_2NiO_{4+\delta}$ in all of the La-deficient samples were slightly higher than the theoretical values. This result further reveals that the $La_2NiO_{4+\delta}$ could not suffer from a high La deficiency. In addition, based on the XRD patterns, the crystal size of $La_3Ni_2O_7$ phase is estimated with the Scherrer equation. The calculated crystal size of $La_3Ni_2O_7$ phase in $La_{1.98}NiO_{4+\delta}$, $La_{1.95}NiO_{4+\delta}$ and $La_{1.90}NiO_{4+\delta}$ is 69 nm, 77 nm and 84 nm, respectively. In the lattice of $La_2NiO_{4+\delta}$ oxide, two types of La may exist: one located in the perovskite layer and the other located in the rock-salt layer. Konysheva et al. proposed that the weak bond energy of the Ni-O bond cannot sustain a large A-site cation deficiency in ABO_3 (B=Ni) perovskite materials.[32] This rule may also be applicable to the perovskite layer(s) in the Ruddlesden-Popper-type $La_2NiO_{4+\delta}$ phase. Then, if the La deficiency occurs in the rock-salt layer, a higher-order RP phase should appear. It then well explains the detection of a $La_3Ni_2O_7$ phase in the La-deficient $La_{2-x}NiO_{4+\delta}$ samples in this study.

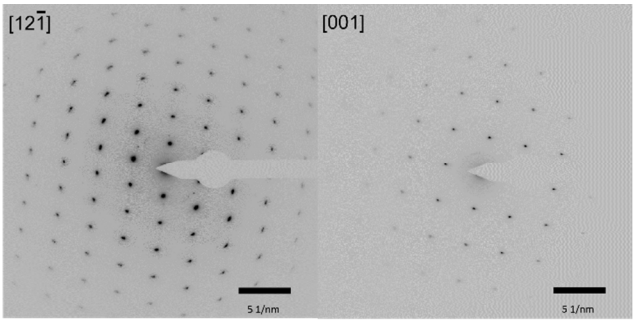

Figure 2 The diffraction patterns recorded by SAED from two different regions for the $La_{1.95}NiO_{4+\delta}$ sample.

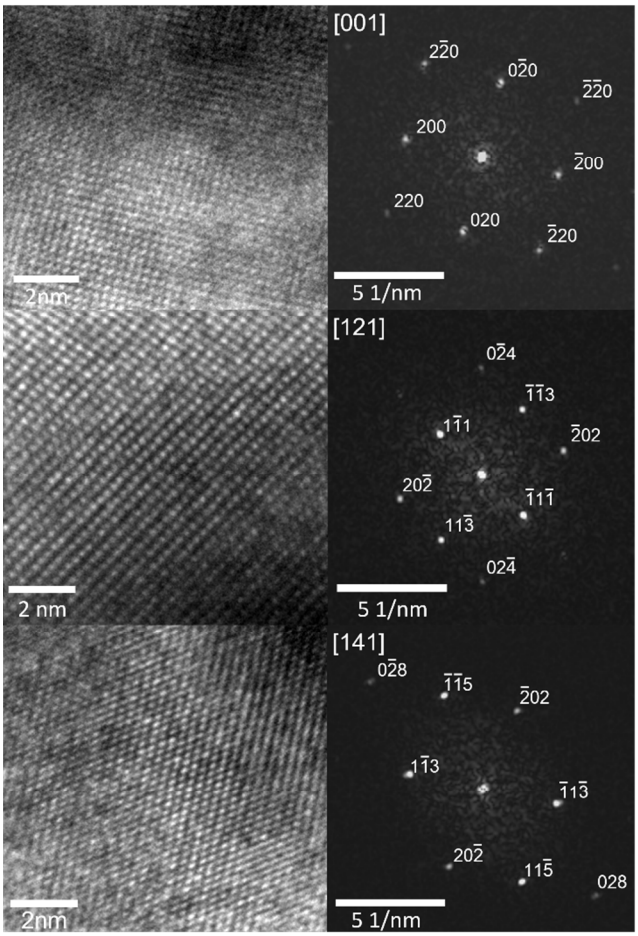

Figure 3 The lattice structure of the $La_{1.95}NiO_{4+\delta}$sample from different orientations, and corresponding diffraction data from FFT of the lattice.

TEM observations were conducted on a $La_2NiO_{4+\delta}$ sample and a $La_{1.95}NiO_{4+\delta}$ sample to obtain further structural information. For the cation-stoichiometric $La_2NiO_{4+\delta}$ sample, the diffraction patterns (Fig. S5b) acquired via FFT related to the region (Fig. S5a) can be indexed to a K_2NiF_4 structure with a space group of F *mmm,* and the orientation is [21-1]. The diffraction patterns recorded by SAED from two different regions of the $La_{1.95}NiO_{4+\delta}$ sample are presented in Fig. 2. The patterns can also be indexed to the $La_2NiO_{4+\delta}$ phase with the orientations of [12-1] and [001], separately. To obtain more detailed structural information of $La_{1.95}NiO_{4+\delta}$, HRTEM observations were conducted. Fig. 3 shows the lattice structure of the $La_{1.95}NiO_{4+\delta}$ sample from different orientations, as well as the corresponding diffraction data from FFT of the lattice. All of the diffraction patterns could be indexed based on the crystal structure of the orthorhombic $La_2NiO_{4+\delta}$ phase. The interplanar spaces measured from the diffraction data were similar to the values calculated from the Rietveld refinement of the X-ray diffractions, and the detailed data are listed in Table S1. More importantly, no cation vacancies were observed from the images. This result unambiguously demonstrates the conclusion derived from the X-ray diffraction analysis, *i.e.*, the La deficiency in $La_2NiO_{4+\delta}$ was negligible, and the La-to-Ni molar ratio of less than 2 will bring about the formation of a high-order $La_3Ni_2O_7$ phase.

The high-ordered $La_3Ni_2O_7$ and $La_4Ni_3O_{10}$ were demonstrated to

show better electrochemical performance and higher electronic conductivity than the cation-stoichiometric $La_2NiO_{4+\delta}$.[33-35] This result suggests an improved electrochemical performance compared with that of a stoichiometric $La_2NiO_{4+\delta}$ phase should be observed for the La-deficient $La_{2-x}NiO_{4+\delta}$ if a high-order Ruddlesden-Popper phase formed. However, this prospect seems controversial to the electrochemical results reported in the literature.[20,21] The electrochemical performances of the various La-deficient $La_{2-x}NiO_{4+\delta}$ oxides as catalysts for ORR were systematically re-examined based on symmetrical cell tests using electrochemical impedance spectroscopy (EIS) in this study. Fig. 4 shows Nyquist plots for symmetrical $La_{2-x}NiO_{4+\delta}$||SDC||$La_{2-x}NiO_{4+\delta}$ cells measured in ambient air from 500 to 750 °C. The impedance spectra show that the polarization resistance monotonously increased as the content of $La_3Ni_2O_7$ increased. More specifically, the polarization resistances of the $La_{1.98}NiO_{4+\delta}$ electrode were slightly higher than those of the $La_2NiO_{4+\delta}$ electrode, whereas the polarization resistance of the $La_{1.95}NiO_{4+\delta}$ electrode increased by approximately 30 % compared with that of $La_2NiO_{4+\delta}$. In addition, the shapes of the impedance spectra for the La-deficient $La_{2-x}NiO_{4+\delta}$ electrodes are slightly different from that of the $La_2NiO_{4+\delta}$ electrode. It seems that the presence of $La_3Ni_2O_7$ in the oxides reduced the ORR activity of the electrode. An equivalent circuit (Fig. S6) of the type L-Ro-(R1||CPE1)-(R2||CPE2)-…-(Ri||CPEi) was adopted to fit the impedance spectra. Herein, L is the inductance from the external devices, Ro is the ohmic resistance, and a series of resistance-constant phase elements (Ri-CPEi) in parallel represents different electrochemical process from high frequency to low frequency in the impedance spectra. At temperatures higher than 600 °C, two (R-CPE) fit the spectra well; however, in the low temperature region, one more (R-CPE) is required to fit an additional semi-arc at the high frequency region. The parameters obtained from the data fitting to the equivalent circuit as a function of temperature for $La_2NiO_{4+\delta}$ are listed in Table 2. For the La-deficient $La_{2-x}NiO_{4+\delta}$ samples, the fitting data are listed in Table S2. The fitted impedance spectra are also presented in Fig. 4.

In a previous study based on a $La_2NiO_{4+\delta}$||YSZ||$La_2NiO_{4+\delta}$ symmetrical cell, the arc at high relaxation frequency was attributed to the transfer of oxygen ions at the electrode/electrolyte interface.[36] Herein, considering the much higher relaxation frequency and smaller capacitance of the first arc, this first process appeared at low temperatures and was more likely to be related to charge transfer around the grain boundary of the SDC electrolyte.[5] On the other hand, the C2 and C3 values associated with the medium and low-frequency arcs fluctuated at approximately 1×10^{-5} and 1×10^{-3}~1×10^{-2} F cm^{-2}, respectively. These two processes with low relaxation frequency and large capacitance should be related to the electrode processes. The resistances belonging to three arcs at high, medium and low frequency were then separately plotted (Fig. S7). It can be seen that the values of R1 from different symmetrical cells are close to each other. In addition the calculated activation energies are also similar to each other at approximately 1.1 eV, which corresponds to the previously reported activation energy for charge transfer around the grain boundary of SDC.[37] This result further confirms that the first arc in the impedance spectra originates from the SDC electrolyte. For R2, which belonged to the arc at intermediate frequency, a distinct increment was observed as the La nonstoichiometry increased, *i.e.*, more $La_3Ni_2O_7$ phase presented in the samples. For R3, which was from the arc at low frequency, its value was insensitive to the presence of the $La_3Ni_2O_7$ phase inside the samples. Therefore, the deteriorated electrode performance was mainly attributed to the increased polarization resistance at the intermediate frequency range.

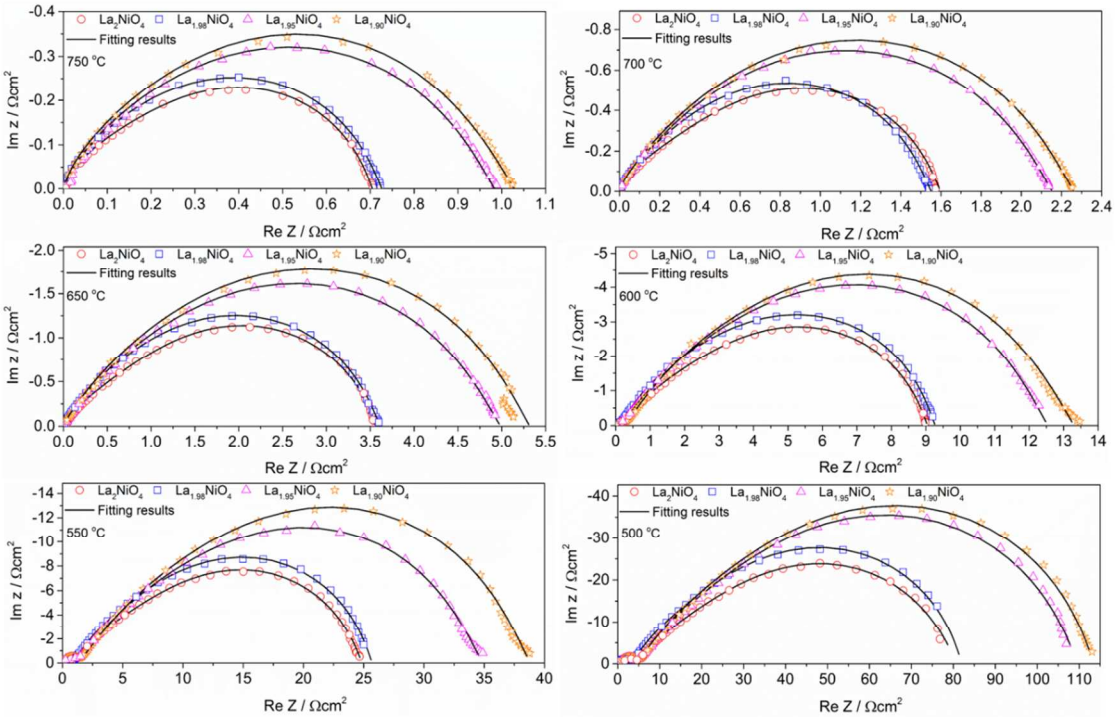

Figure 4 Nyquist plots for symmetrical $La_{2-x}NiO_{4+\delta}$||SDC||$La_{2-x}NiO_{4+\delta}$ cells measured in ambient air from 500 to 750 °C.

Table 2 The parameters obtained from the data fitting to the equivalent circuit as a function of temperature for $La_2NiO_{4+\delta}$

$La_2NiO_{4+\delta}$	Temperature(℃)	750	700	650	600	550	500
Arc1	R1 (Ω cm^2)	/	/	/	0.5724	1.483	3.276
	C1 (F cm^{-2})	/	/	/	7.589E-10	1.113E-10	5.63E-9
	f1 (Hz)	/	/	/	3.664E8	9.644E8	8.626E6
Arc2	R2 (Ω cm^2)	0.2930	0.5932	1.410	3.525	10.623	35.1
	C2 (F cm^{-2})	3.609E-5	1.122E-5	7.05E-6	2.488E-5	1.859E-5	6.58E-6
	f2 (Hz)	15051	23912.5	16013.4	1814.5	806.0	688.7
Arc3	R3 (Ω cm^2)	0.4308	1.0326	2.2146	5.325	13.26	41.5
	C3 (F cm^{-2})	0.002926	0.00237	0.00303	0.004823	0.00757	0.00872
	f3 (Hz)	126.27	65.17	23.736	6.197	1.585	0.44

To obtain additional information regarding the electrochemical processes involved in the electrode, the influence of oxygen partial pressure (0.05~0.4 atm) on the impedance spectra of the symmetrical cell with $La_2NiO_{4+\delta}$ as the electrode from 550 °C to 700 °C was measured and fitted. An equivalent circuit with three (R-CPE) units was required to fit the data at 550 °C, and an equivalent circuit with two (R-CPE) units was necessary for the data at higher temperatures. Because the first arc in the spectra was attributed to the electrolyte within the oxygen partial pressure range of 0.05-0.4 atm, the resistance for the first arc, which originated from electrolyte grain boundary and was observable at 550 °C, was set to a constant value when fitting the EIS data. From the fitting parameters listed in Table S3, it can be found that the orders of magnitude of the characteristic capacitances and relaxation frequencies in different arcs at high-temperature points are similar to those obtained from the low-temperature points. This result reveals that the rate-determining step at each process did not change as the test temperature varied.

In general, the polarization resistance of an electrode is dependent on the oxygen partial pressure of the surrounding atmosphere, and it usually follows the following relationship: $\frac{1}{R_p} \propto P_{O_2}^m$. Different rate-determining steps in an oxygen reduction process in the electrode are represented by different m values. For example, the m values are 1, 0.5, 0.25 and 0 when the rate-determining step is the adsorption of molecular oxygen at the electrode surface ($O_2(g) \leftrightarrow O_{2,ads}$), the dissociation of molecular oxygen ($O_{2,ads} \leftrightarrow 2O_{ads}$), the charge transfer process ($O_{ads} + 2e^- + V_O^{\cdot\cdot} \leftrightarrow O_O^X$), and the transfer of oxygen ions at the electrode/electrolyte interface, respectively.[38] However, it is often difficult to separate the latter two processes (m=0.25 and 0) from the EIS because their characteristic frequencies are typically close to each other.[39] The dependence of polarization resistances at medium (R2) and low (R3) frequencies on oxygen partial pressure is displayed in Fig. 5. From 550 to 700 °C, the m values were, in order, 0.26, 0.30, 0.33 and 0.34 for R2. For R3, the m values at 550, 600, 650 and 700 °C increased to 0.45, 0.44, 0.44 and 0.43, respectively. Generally, the m values for R2 are approximately 0.3, and the values for R3 are close to 0.5. Considering the low capacitance for R2 at approximately 10^{-5} F cm^{-2} and the high capacitance of 10^{-1} F cm^{-2} for R3, it is reasonable to ascribe the arc at medium frequency to the charge transfer process occurring at the electrode/gas interface and/or oxygen ions transferring through the electrolyte/electrode interface. The rest arc at low frequency should be due to the dissociation of molecular oxygen at the electrode surface. In combination with the above-mentioned gradually increased R2 value due to the La deficiency, it can be concluded that the presence of $La_3Ni_2O_7$ was detrimental to the charge transfer process in $La_2NiO_{4+\delta}$ electrodes. This conclusion is somewhat unexpected because the electrode electrical conductivity should be enhanced due to the high electrical conductivity of $La_3Ni_2O_7$, and the oxygen reduction activity should improve due to the good electrochemical performance of $La_3Ni_2O_7$.

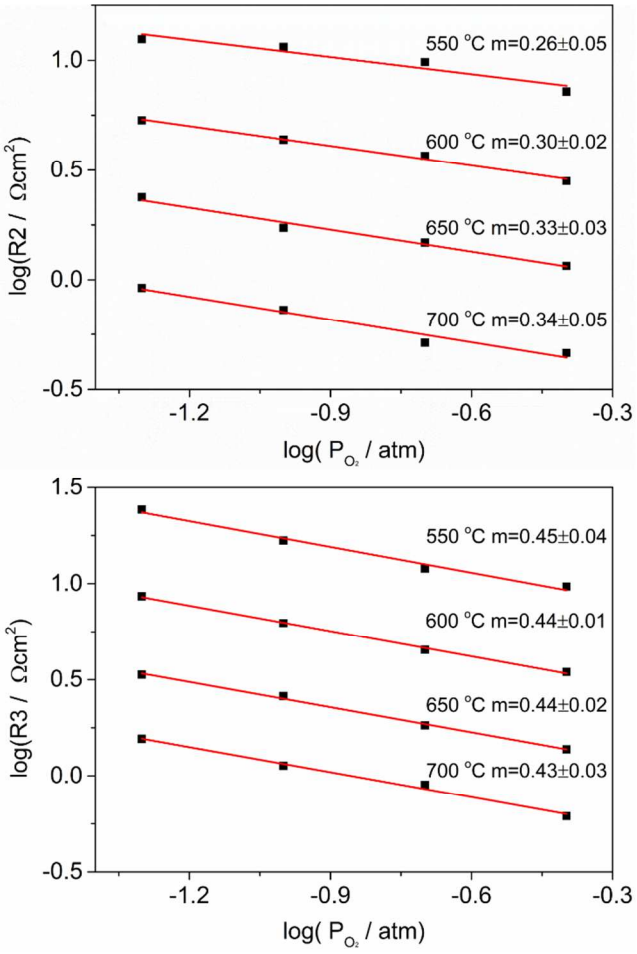

Figure 5 The dependence of polarization resistances at medium (R2) and low (R3) frequencies on oxygen partial pressure.

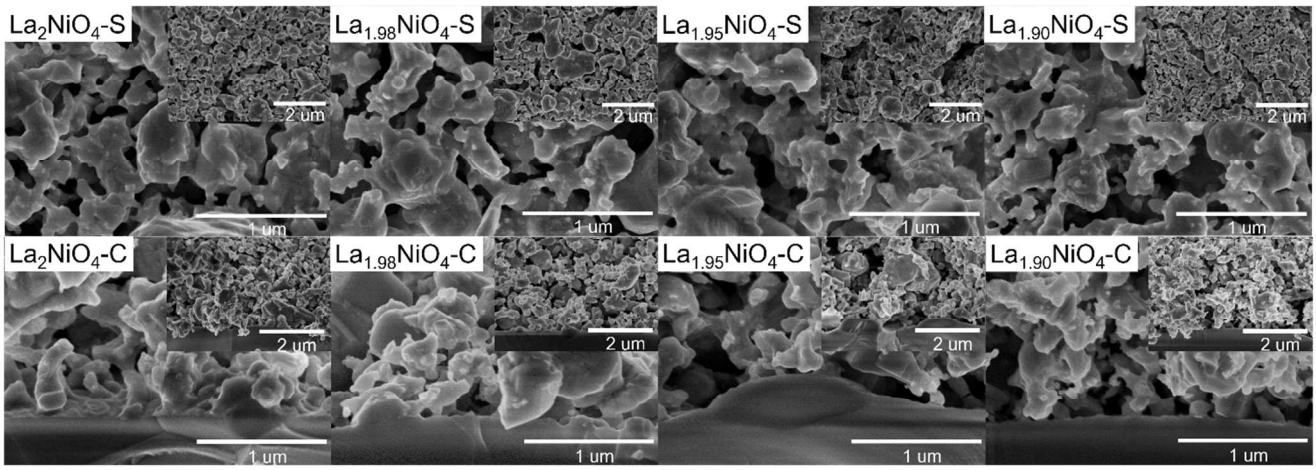

Figure 6 The microstructures of all electrodes from both surface ($La_{2-x}NiO_{4+\delta}$-S) and cross-section ($La_{2-x}NiO_{4+\delta}$-C) views.

It was reported that $La_3Ni_2O_7$ had poor sintering ability compared with $La_2NiO_{4+\delta}$.[34] The formation of $La_3Ni_2O_7$ in the La-deficient $La_{2-x}NiO_{4+\delta}$ samples might prohibit the formation of a well-connected electrode architecture, thus introducing blocks for charge transfer between individual grains in the electrode. The microstructures of these electrodes with different degrees of La deficiency were then examined using SEM, as presented in Fig. S8. First, the situations of elemental distribution of the three La-nonstoichiometric $La_{2-x}NiO_{4+\delta}$. electrodes were detected, and good uniformity of these electrodes was confirmed by SEM-EDS. This result reveals that the $La_3Ni_2O_7$ phase and the $La_2NiO_{4+\delta}$ phase were uniformly mixed. Then, the microstructures of all of the electrodes were carefully examined from both surface and cross-section views using the images shown in Fig. 6. From the images of the surface microstructures of the $La_{2-x}NiO_{4+\delta}$ electrodes, all of the electrodes exhibited porous structures and should be sufficient for gas diffusion. As the content of $La_3Ni_2O_7$ increased, the porosity did not vary greatly. However, more small particles were observed, and the particle interconnections were poor. From the cross-sectional view, a clear change in the interconnection between the electrode and the electrolyte was observed.

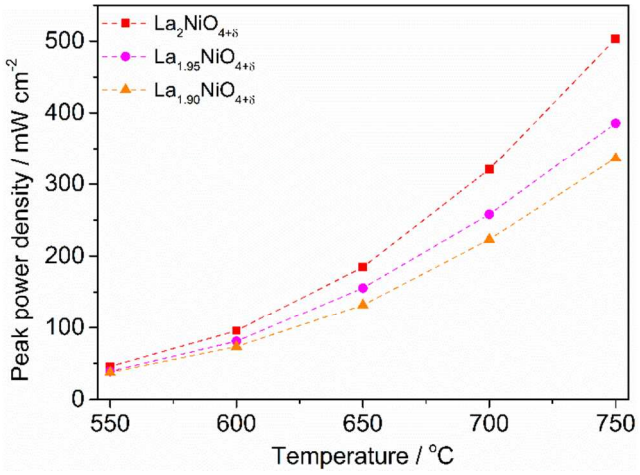

Figure 7 the power outputs of single cells with $La_{2-x}NiO_{4+\delta}$ materials as cathodes.

For the $La_2NiO_{4+\delta}$ and $La_{1.98}NiO_{4+\delta}$ electrodes, their electrode layers were both well adhered to the SDC electrolyte. However, the interconnection quality decreased as the La nonstoichiometry increased and was likely caused by the poor sintering ability of the $La_3Ni_2O_7$ phase. From the EIS analysis, the deteriorated electrochemical performance in La-deficient $La_{2-x}NiO_{4+\delta}$ electrodes was attributed to the affected charge transfer process and/or oxygen ions transferring through the electrolyte/electrode interface. Both of these two processes were reported to have strong relation to the electrode microstructure.[40] Therefore, the poor particle interconnection in the electrode layer and the poor physical contact between the electrode and the electrolyte should be responsible for the worse electrochemical performance of these La-deficient $La_{2-x}NiO_{4+\delta}$ electrodes. In summary, although the $La_3Ni_2O_7$ phase in the $La_{2-x}NiO_{4+\delta}$ electrode had high electrical conductivity and good electrochemical performance, its poor sintering ability was detrimental to the electrochemical performance of the La-deficient $La_{2-x}NiO_{4+\delta}$ electrode. This result explains why no performance improvements were observed for the La-deficient $La_{2-x}NiO_{4+\delta}$ materials.

Finally, the power outputs of single cells with $La_{2-x}NiO_{4+\delta}$ materials as cathodes were tested to study the influence of the $La_3Ni_2O_7$ phase on the performance of the $La_{2-x}NiO_{4+\delta}$ materials in actual single cells. The trends of the power outputs are shown in Fig. 7, and the *I-V* curves are presented in Fig. S9. Peak power densities of 503, 321, 185, 96 and 46 mW cm^{-2} were obtained for the cell with a $La_2NiO_{4+\delta}$ cathode. For the fuel cells with either $La_{1.95}NiO_{4+\delta}$ or $La_{1.90}NiO_{4+\delta}$ as cathodes, relatively low power outputs were obtained, as expected. This result corresponds to the poor electrochemical performance of $La_{1.95}NiO_{4+\delta}$ or $La_{1.90}NiO_{4+\delta}$ electrodes, as demonstrated in the symmetrical cell tests.

Conclusions

In summary, the potential to introduce La deficiency into a Ruddlesden-Popper-type $La_2NiO_{4+\delta}$ material and its effect on the electrode performance for oxygen reduction reaction was explored in the current study. The tolerance to La deficiency in the $La_2NiO_{4+\delta}$ structure was found to be very low, which should be related to the weak Ni-O bond energy in the perovskite layer.

Instead, a high-order $La_3Ni_2O_7$ phase was preferentially produced in nominal La-deficient $La_{2-x}NiO_{4+\delta}$ materials. Despite the higher electrical conductivity and improved electrochemical performance of $La_3Ni_2O_7$, its poor sintering ability prohibited the sintering of the electrode onto the electrolyte and the framework of the electrode itself. As a result, degraded electrode performances were observed for the nominal La-deficient $La_{2-x}NiO_{4+\delta}$ electrodes. Therefore, the strategy of introducing La deficiency in $La_2NiO_{4+\delta}$ to enhance its electrochemical performance is impractical, whereas improving the sintering ability of $La_2NiO_{4+\delta}$ and related materials should be a more practical method to promote their electrochemical performance. In addition, the phase composition may vary for $Pr_2NiO_{4+\delta}$ and $Nd_2NiO_{4+\delta}$ materials that have similar structures when Pr/Nd deficiency is deliberately created; thus, further studies are necessary.

Experimental

Powder preparation

$Ce_{0.8}Sm_{0.2}O_{1.9}$ (SDC) was used as the electrolyte in this study. All of the $La_{2-x}NiO_{4+\delta}$ (x=0, 0.02, 0.05 and 0.1) and SDC oxide powders were synthesized via a combined EDTA-citrate-complexing sol-gel method. Analytical grade $La(NO_3)_3{\cdot}6H_2O$, $Ni(NO_3)_2{\cdot}6H_2O$, $Ce(NO_3)_4{\cdot}6H_2O$ and $Sm(NO_3)_3$ were used as the raw materials. For a typical synthesis process, stoichiometric amounts of raw materials were weighed and dissolved into deionized water. Then, EDTA and citrate were sequentially added to the solution at a molar ratio of 1:1.5. The solution mixture was stirred under heating until a gel formed, which was then heated at 240 °C for ~5 h to obtain a solid precursor. The precursor was further calcined in air at 1100 °C for 24 h ($La_{2-x}NiO_{4+\delta}$) or at 800 °C for 5 h (SDC) to obtain the final product.

Fuel cell fabrication

To prepare electrode slurries, the $La_{2-x}NiO_{4+\delta}$ powders were first dispersed in a premixed solution of glycol (0.6 mL), ethylene glycol (2 mL) and isopropyl (10 mL) to form the slurries. The slurries were then milled using a high-energy ball miller (Fritsch, Pulverisette 6) at a rotational speed of 400 rpm for 30 min to obtain the final electrode slurries.

Symmetrical cells with SDC as the electrolytes were fabricated for electrode impedance tests. Dense SDC membranes with a diameter of ~12 mm were prepared through a dry pressing method. Then, the electrode slurries were spray-deposited onto both sides of the SDC electrolytes. To form the symmetrical cells, the deposited electrodes were sintered at 1000 °C for 2 h in ambient air. To avoid the influence of the possible catalytic activity of silver, a diluted gold paste was used as the current collector.[41] The electrode morphologies were studied using an FE-SEM (HITACHI S-4800), and EDS scanning was performed using an E-SEM (FEI Quanta-200). Single SOFC test cells were fabricated based on type-casting anode-supported half-cells with the structure of YSZ+NiO||YSZ||SDC||$La_{2-x}NiO_{4+\delta}$. The process used to prepare the electrode of the symmetrical cell was used to prepare the cathode layer. The effective area of the cathode was 0.48 cm^2.

Characterization

The obtained samples were characterized using RT powder X-ray diffraction technique for phase composition identification. A diffractometer (Rigaku Smartlab, Cu Kα radiation, λ = 1.5418 Å) in the Bragg-Brentano reflection geometry was used. The diffraction patterns were recorded by continuous scanning in the 2θ range of 20-90 ^{o} with an interval of 0.02 ^{o}. The obtained diffraction profiles were analyzed using the Rietveld method with the GSAS program and EXPGUI interface.[42] During the refinement, the parameters of the scale factor, lattice parameters, peak shape (pseudo-Voigt function), background and isotropic atomic displacement parameters were refined. Transmission electron microscopy (TEM) was performed using an FEI Tecnai T30F instrument.

The electrochemical impedance spectra of the $La_{2-x}NiO_{4+\delta}$ electrodes were measured using an electrochemical workstation composed of a 1260 frequency response analyzer and a Solartron 1287 potentiostate. The symmetrical cells were placed in a quartz tube reactor with controllable oxygen partial pressure (mix O_2 with N_2 using mass flow controllers). The frequency range of the electrochemical impedance spectroscopy measurement was from 0.1-0.01 Hz to 1 MHz with a signal amplitude of 10 mV. The samples were tested under an open circuit voltage condition. The spectra were fitted by a complex non-linear least squares fitting program using ZView software. The single cells were connected to a digital sourcemeter (Keithley 2420) using silver wires to characterize the electrochemical performance.

Acknowledgements

This work was supported by the Key Projects in Nature Science Foundation of Jiangsu Province under contract no. BK2011030, by the National Science Foundation for Distinguished Young Scholars of China under contract no. 51025209, by the "National Nature Science Foundation of China" under contract no. 21103089, and by the Priority Academic Program Development of Jiangsu Higher Education Institutions(PAPD).

Notes and references

[a] *State Key Laboratory of Materials-Oriented Chemical Engineering, College of Chemistry & Chemical Engineering, Nanjing Tech University, Nanjing 210009, China*

[b] *Department of Mechanical and Aerospace Engineering, The Hong Kong University of Science and Technology, Hong Kong, SAR China.*

[c] *College of Energy, Nanjing Tech University, Nanjing 210009, China*

† Electronic Supplementary Information (ESI) available: Fitting paramaters of and impedace spectra; Refined X-ray diffraction patterns; I-V curves of single cells. See DOI: 10.1039/b000000x/

1. R. M. Ormerod, *Chem. Soc. Rev.*, 2003, **32**, 17.
2. D. J. Brett, A. Atkinson, N. P. Brandon and S. J. Skinner, *Chem. Soc. Rev.*, 2008, **37**, 1568.
3. B. C. Steele and A. Heinzel, *Nature*, 2001, **414**, 345.
4. Z. Shao and S. M. Haile, *Nature*, 2004, **431**, 170.
5. D. Chen, R. Ran, K. Zhang, J. Wang and Z. Shao, *J. Power Sources*, 2009, **188**, 96.
6. E. Bucher, M. Yang and W. Sitte, *J. Electrochem. Soc.*, 2012, **159**, B592.
7. N. H. Menzler, D. Sebold and E. Wessel, *J. Power Sources*, 2014, **254**, 148.

8. A. Yan, M. Cheng, Y. Dong, W. Yang, V. Maragou, S. Song and P. Tsiakaras, *Appl. Catal., B*, 2006, **66**, 64.
9. N. Arulmozhi, W. H. Kan, V. Thangadurai and K. Karan, *J. Mater. Chem. A*, 2013, **1**, 15117.
10. W. Jung and H. L. Tuller, *Energy Environ. Sci.*, 2012, **5**, 5370.
11. Y. Chen, W. Jung, Z. Cai, J. J. Kim, H. L. Tuller and B. Yildiz, *Energy Environ. Sci.*, 2012, **5**, 7979.
12. Z. Feng, Y. Yacoby, M. J. Gadre, Y. L. Lee, W. T. Hong, H. Zhou, M. D. Biegalski, H. M. Christen, S. B. Adler, D. Morgan and S. H. Yang, *J. Phys. Chem. Lett.*, 2014, **5**, 1027.
13. M. J. Gadre, Y. L. Lee and D. Morgan, *Phys. Chem. Chem. Phys.*, 2012, **14**, 2606.
14. J. W. Han and B. Yildiz, *Energy Environ. Sci.*, 2012, **5**, 8598.
15. J. C. Grenier, A. Wattiaux, J. P. Doumerc, P. Dordor, L. Fournes, J. P. Chaminade and M. Pouchard, *J. Solid State Chem.*, 1992, **96**, 20.
16. P. Ganguly and C. N. R. Rao, *J. Solid State Chem.*, 1984, **53**, 193.
17. A. Tarancón, M. Burriel, J. Santiso, S. J. Skinner and J. A. Kilner, *J. Mater. Chem.*, 2010, **20**, 3799.
18. V. V. Kharton, A. V. Kovalevsky, M. Avdeev, E. V. Tsipis, M. V. Patrakeev, A. A. Yaremchenko, E. N. Naumovich and J. R. Frade, *Chem. Mater.*, 2007, **19**, 2027.
19. Y. Wang, X. Zhao, S. Lü, B. Yu, X. Meng, Y. Zhang, J. Yang, C. Fu and Y. Ji, *Ceram. Int.*, 2014, **40**, 7321.
20. H. Zhao, F. Mauvy, C. Lalanne, J. Bassat, S. Fourcade and J. Grenier, *Solid State Ionics*, 2008, **179**, 2000.
21. M. Ferkhi, A. Ringuedé, A. Khaled, L. Zerroual and M. Cassir, *Electrochim. Acta*, 2012, **75**, 80.
22. J. Xie, Y.-W. Ju, M. Matsuka, S. Ida and T. Ishihara, *J. Power Sources*, 2013, **228**, 229.
23. V. Sadykov, Y. Okhlupin, N. Yeremeev, Z. Vinokurov, A. Shmakov, V. Belyaev, N. Uvarov and J. Mertens, *Solid State Ionics*, 2014, **262**, 918.
24. F. Mauvy, C. Lalanne, J. M. Bassat, J. C. Grenier, A. Brisse, A. L. Sauvet, C. Barthet and J. Fouletier, *Solid State Ionics*, 2009, **180**, 1183.
25. C. Lalanne, G. Prosperi, J. Bassat, F. Mauvy, S. Fourcade, P. Stevens, M. Zahid, S. Diethelm, J. Vanherle and J. Grenier, *J. Power Sources*, 2008, **185**, 1218.
26. H. Luebbe, J. Van herle, H. Hofmann, P. Bowen, U. Aschauer, A. Schuler, F. Snijkers, H.-J. Schindler, U. Vogt and C. Lalanne, *Solid State Ionics*, 2009, **180**, 805.
27. E. Boehm, J. Bassat, P. Dordor, F. Mauvy, J. Grenier and P. Stevens, *Solid State Ionics*, 2005, **176**, 2717.
28. M. Zinkevich and F. Aldinger, *J. Alloys Compd.*, 2004, **375**, 147.
29. P. Odier, Y. Nigara, J. Coutures and M. Sayer, *J. Solid State Chem.*, 1985, **56**, 32.
30. A. Aguadero, J. A. Alonso, M. J. Martinez-Lope, M. T. Fernandez-Diaz, M. J. Escudero and L. Daza, *J. Mater. Chem.*, 2006, **16**, 3402.
31. R. Sayers, J. E. Parker, C. C. Tang and S. J. Skinner, *J. Mater. Chem.*, 2012, **22**, 3536.
32. E. Y. Konysheva, X. Xu and J. T. Irvine, *Adv. Mater.*, 2012, **24**, 528.
33. G. Amow, I. Davidson and S. Skinner, *Solid State Ionics*, 2006, **177**, 1205.
34. G. Amow and S. J. Skinner, *J. Solid State Electrochem.*, 2006, **10**, 538.
35. S. Takahashi, S. Nishimoto, M. Matsuda and M. Miyake, *J. Am. Ceram. Soc.*, 2010, **93**, 2329.
36. M. J. Escudero, A. Aguadero, J. A. Alonso and L. Daza, *J. Electroanal. Chem.*, 2007, **611**, 107.
37. Z. Zhan, T.-L. Wen, H. Tu and Z.-Y. Lu, *J. Electrochem. Soc.*, 2001, **148**, A427.
38. Y. Takeda, R. Kanno, M. Noda, Y. Tomida and O. Yamamoto, *J. Electrochem. Soc.*, 1987, **134**, 2656.
39. M. J. Jørgensen and M. Mogensen, *J. Electrochem. Soc.*, 2001, **148**, A433.
40. D. Chen, R. Ran and Z. Shao, *J. Power Sources*, 2010, **195**, 4667.
41. R. Sayers and S. J. Skinner, *J. Mater. Chem.*, 2011, **21**, 414.
42. B. H. Toby, *J. Appl. Crystallogr.*, 2001, **34**, 210.

$La_2NiO_{4+\delta}$ is proved that it cannot tolerate a high La-deficiency for the first time. The catalytic performance of nominal La-deficient $La_2NiO_{4+\delta}$ is poor due to the presence of $La_3Ni_2O_7$ phase.